PHYSICAL REVIEW E **00**, 006300 (2012)

Analytical solutions of drying in porous media for gravity-stabilized fronts

A. G. Yiotis and D. Salin
Laboratoire FAST, Université Pierre & Marie Curie, Université d'Orsay Paris-Sud, CNRS, Orsay 91405, France

E. S. Tajer and Y. C. Yortsos
Mork Family Department of Chemical Engineering and Materials Science, University of Southern California,
Los Angeles, California 90089-1450, USA

(Received 17 June 2011; revised manuscript received 11 January 2012; published xxxxx)

We develop a mathematical model for the drying of porous media in the presence of gravity. The model incorporates effects of corner flow through macroscopic liquid films that form in the cavities of pore walls, mass transfer by diffusion in the dry regions of the medium, external mass transfer over the surface, and the effect of gravity. We consider two different cases: when gravity opposes liquid flow in the corner films and leads to a stable percolation drying front, and when it acts in the opposite direction. In this part, we develop analytical results when the problem can be cast as an equivalent continuum and described as a one-dimensional (1D) problem. This is always the case when gravity acts against drying by opposing corner flow, or when it enhances drying by increasing corner film flow but it is sufficiently small. We obtain results for all relevant variables, including drying rates, extent of the macroscopic film region, and the demarkation of the two different regimes of constant rate period and falling rate period, respectively. The effects of dimensionless variables, such as the bond number, the capillary number, and the Sherwood number for external mass transfer are investigated. When gravity acts to enhance drying, a 1D solution is still possible if an appropriately defined Rayleigh number is above a critical threshold. We derive a linear stability analysis of a model problem under this condition that verifies front stability. Further analysis of this problem, when the Rayleigh number is below critical, requires a pore-network simulator which will be the focus of future work.

DOI: 10.1103/PhysRevE.00.006300 PACS number(s): 47.56.+r, 68.03.Fg

I. INTRODUCTION

During the drying of a porous medium, initially fully saturated by a volatile liquid, evaporation gives rise to a number of liquid-gas interfaces. These are located in pore bodies, that define the percolation front [Fig. 1(d)], but also reside in the cavities and corners along the pore walls in the form of macroscopic liquid films, which develop as the bulk liquid-gas menisci recede in the pore space [Figs. 1(b)–1(c)]. The movement of these interfaces is controlled by the combined action of capillary, gravity, and viscous forces.

As in all drainage processes, fluid transport through the liquid films is an important transport mechanism. Films provide hydraulic connectivity between liquid-saturated regions that may appear to be macroscopically disconnected [1,2]. Such flows are induced by capillarity and driven by changes in the curvature of the liquid-gas menisci [3,4]. These macroscopic films should be clearly distinguished from thin films that develop on flat surfaces of the pore walls as vapor molecules are absorbed due to van der Waals forces. Liquid flow through the latter thin films, as well as mass transfer by diffusion in the film region, has been shown to be negligible compared to corner flow in the cavities through macroscopic films [5].

Recent drying studies have suggested that macroscopic films provide hydraulic connectivity even at late times when a significant amount of the liquid has evaporated [6–8]. If the films reach the external surface S of the medium, wicking action keeps the surface at least partially wet. As more films get detached, the liquid content at the surface progressively decreases. However, the surface remains saturated with the evaporating species, even at small liquid content (liquid saturation), provided that the thickness of the external mass transfer boundary layer is sufficiently larger than the characteristic pore size of the medium [9]. Under such conditions, the process is controlled by mass transfer through the boundary layer and characterized by a constant drying rate [the constant rate period (CRP) regime], which may last up to very late times [8,10].

At a certain length, liquid films cannot sustain capillary flow over increasingly larger lengths and they become detached [6,11–13]. Then, a completely dry region (absence of bulk liquid and corner flow through macroscopic films) develops between the evaporation front and the external surface. Drying is now controlled by diffusion through this dry region and the evaporation rate starts decreasing signaling the onset of the falling rate period (FRP) [Fig. 1(d)].

Previous studies have explored in detail various mathematical models of drying, including those based on a pore-network representation of the porous medium (developed by Fatt [14]). These have progressed from simple percolation models [15,16], to models that include corner film flow [17,18], and more recently those incorporating the effect of an external mass transfer boundary layer [10]. Absent has been the effect of gravity, which in many applications can play an important role. Indeed, in recent experiments [19–21] it was found that incorporating gravity in drying is necessary to match the experimental results. It is the objective of our work to address the effect of gravity in the drying of porous media and quantities such as film extent, film thickness, and drying rates.

In this paper we develop the mathematical formalism to incorporate the effect of gravity. This can be stabilizing or destabilizing, depending on the orientation of the porous medium [stabilizing when gravity opposes corner flow in the films (and thus drying) and destabilizing in the opposite case, assuming sufficiently strong buoyancy]. We provide analytical solutions for relevant quantities when gravity opposes drying and investigate the sensitivity to dimensionless variables, such as the bond number, the capillary number, and the Sherwood number. Attention is paid to drying curves and the conditions that mark the transition between the constant (CRP) and the falling rate (FRP) periods. When gravity enhances corner film flow, an equivalent 1D continuum can still apply if a critical threshold for an equivalent Rayleigh number is exceeded. We derive such a condition and infer its validity by a simplified stability analysis. For the more general case, a detailed pore-network is needed. This is a subject for future research [21].

II. MODEL FORMULATION

As in our previous studies [10,11,17], we postulate the following [Fig. 1(d)]: An external mass transfer boundary layer over the external surface S of the porous medium (sometimes referred to as the product surface), where the evaporating species is purged; an innermost region of pores, fully occupied by liquid (liquid saturated region); and intermediate regions containing pores partly occupied by liquid films (film region) or not occupied at all (dry region), depending on the extent of the process. The interface between the fully occupied and film pores is typically a percolation front (which in the presence of gravity can be determined using invasion percolation in the presence of a stabilizing or a destabilizing gradient [22,23] depending on the orientation). Gravity modifies both the morphology of the percolation front, as well as the extent of the film region by either enhancing or opposing corner flow in the films. To understand its effects we consider that the full problem can be cast as a 1D equivalent of drying from a material bearing the geometrical characteristics of capillaries with noncircular (i.e., rectangular) cross sections. This allows for the modeling of corner flow in the form of films that develop as the bulk liquid-gas meniscus recedes deeper in the pore space [Figs. 1(a)–1(c)] [19].

Within the film region the dominant mass transport mechanism is corner liquid flow through the films [5]. The films are then parametrized by the radius of curvature of the liquid-gas menisci $r(x,t)$ along their length from the product surface S [11], taken at $\xi = 0$, to the percolation front, taken at an average position $\xi_p < 0$. Under capillary equilibrium, the excess pressure in the film is

$$P_l = -\gamma/r, \tag{1}$$

where γ is the interfacial tension and flow is unidirectional along direction x and described by a Poiseuille-type law [3,4]

$$Q_x = -\frac{C^*r^4}{\mu\beta}\left(\frac{\partial P_l}{\partial x} - \rho_l g_x\right). \tag{2}$$

Here μ is viscosity, g_x is the gravity component, ρ_l is density, β is the dimensionless flow resistance [3], C^*r^2 is the cross sectional area of the liquid film and C^* is a shape factor that expresses the area available for fluid flow in the corners of the capillaries. For the case of a square cross section $C^* = 4 - \pi$. While valid for any gravity orientation [21], this paper will be restricted only to the case when the x direction is aligned with the gravity vector, namely $g_x = \pm g$. Taking into account Eq. (1), the above can be rewritten as

$$Q_x = -\frac{C^*\gamma}{3\mu\beta}\frac{\partial r^3}{\partial x} + \frac{C^*r^4}{\mu\beta}\rho_l g_x. \tag{3}$$

The mass balance for the evaporating species along the capillary is

$$\frac{\partial V}{\partial t} = -\frac{\partial Q_x}{\partial x} - Q_{\mathrm{ev}}, \tag{4}$$

where $V = C^*r^2$, $Q_{\mathrm{ev}} = -(2\pi r D_M/\rho_l)C_e/r_0[\partial\zeta/\partial n]$ is the evaporation rate in a cross section of the capillary, r_0 is the average size of the capillary in the cross section, D_M is the molecular diffusivity, C_e is the equilibrium mass concentration, and $\zeta = C/C_e$ is the dimensionless concentration. n is the normal to the interface and the brackets denote an average over the dimensionless concentration gradient at the interface. The above expression will not be used further, however. In the following we will focus on two distinct macroscopic regions: one in which the gas phase is practically saturated by vapor and transport is through film flow only, and another ahead of the film region, where the pore space is completely dry and the transport is by diffusion in the gas phase only. A macroscopic mass balance will connect the two regions.

In dimensionless notation, this further reads

$$2\mathrm{Ca}_f\frac{C^*\rho_l}{\pi C_e}\frac{\partial\rho}{\partial\tau} = \frac{1}{\rho}\frac{\partial^2\rho^3}{\partial\xi^2} - \frac{3\mathrm{Bo}_x}{\rho}\frac{\partial\rho^4}{\partial\xi} - 2\mathrm{Ca}_f(1-\zeta) \tag{5}$$

where we introduced the dimensionless film thickness $\rho = r/r_0$ (not to be confused with the density notation), length $\xi = x/r_0$, and time $\tau = tD_M/r_0^2$, and we defined the dimensionless capillary and bond numbers

$$\mathrm{Ca}_f = \frac{3\beta\pi\mu D_M C_e}{C^*\gamma\rho_l r_0}, \quad \mathrm{Bo} = \frac{\rho_l g r_0^2}{\gamma}. \tag{6}$$

In our notation, the x direction is always taken from the inside of the porous medium toward the external surface, therefore $\mathrm{Bo}_x = -\mathrm{Bo}$ corresponds to evaporation from the top (gravity-opposed drying), while $\mathrm{Bo}_x = \mathrm{Bo}$ corresponds to evaporation from the bottom (gravity-enhanced drying).

Proceeding with the conventional quasi-steady-state assumption and also considering that evaporation practically occurs only near the film tip (due to the saturated gas phase along the capillary) [11,17], the mass balance simplifies to

$$\frac{\partial q_x}{\partial\xi} = \frac{\partial^2\rho^3}{\partial\xi^2} - 3\mathrm{Bo}_x\frac{\partial\rho^4}{\partial\xi} = 0. \tag{7}$$

The above formalism can also be generalized (e.g., to a pore network). Its continuum equivalent reads

$$\nabla^2\left(\rho^3 - 3\mathrm{Bo}_x\int_0^\xi \rho^4 d\xi\right) = -3\mathrm{Bo}_x\left(\frac{\partial^2}{\partial u^2}\int_0^\xi \rho^4 d\xi + \frac{\partial^2}{\partial\omega^2}\int_0^\xi \rho^4 d\xi\right), \tag{8}$$

where $u = y/r_0$ and $\omega = z/r_0$. When the right-hand side of Eq. (8) is negligible, as in the specific case here of a 1D

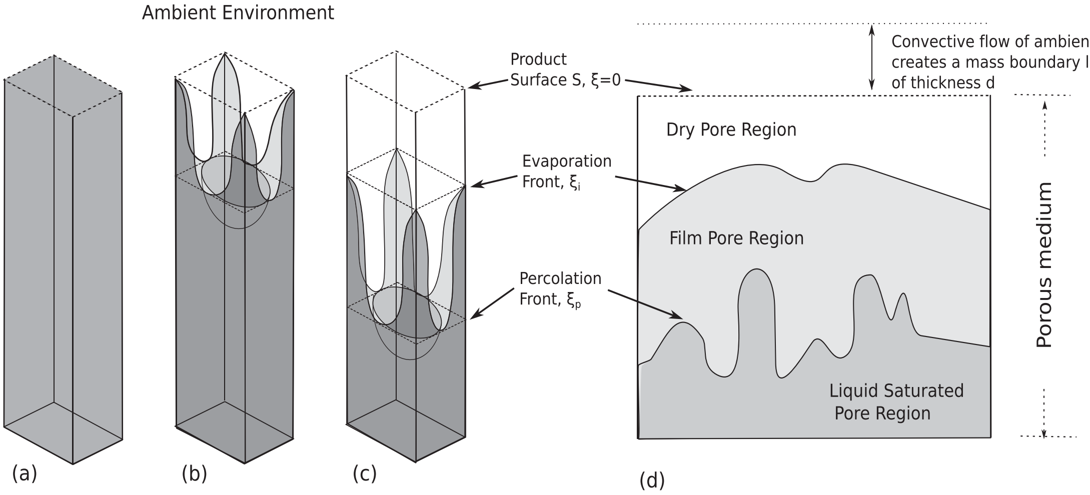

FIG. 1. Schematics of drying from a capillary with a noncircular (i.e., square) cross section with the top side open to the ambient environment (a)–(c). The capillary is initially filled with a volatile liquid up to a certain height (a) (contact angle not shown here). As the liquid evaporates, the liquid-gas interface recedes in the capillary forming a meniscus, while liquid films develop at the corners of the capillary. Initially, the film tips reach up to the initial position of the liquid-gas interface (b). At later times, the film tips depin from their initial position and they recede deeper in the capillary following the movement of the bulk meniscus (c). Also shown in (d) later times of the more general drying problem from a porous medium bounded by an external mass boundary layer of thickness d over the product surface S. The pores can be classified in analogy with the single capillary problem as: (i) completely dry (dry region) where mass transfer is by diffusion only, (ii) pores invaded by the gas phase that contain liquid films at the pore walls (film region) where mass transfer is primarily through corner film flow, and (iii) pores that are fully saturated by the liquid phase (liquid saturated region). The evaporation front (film tips), ξ_i, is located at the interface between the dry and film regions. The percolation front, ξ_p, is located at the interface between film and liquid saturated regions. Lengths are in dimensionless notation.

continuum, we can write

$$\nabla^2\left(\rho^3 - 3\mathrm{Bo}_x\int_0^{\xi}\rho^4 d\xi\right) = 0, \tag{9}$$

the 1D equivalent of which is Eq. (7). Checking the validity of this assumption in the pore-network simulations is a subject for future research [21].

In the dry region (where $\rho = 0$), the mass balance at steady state is the Laplace equation

$$\nabla^2\zeta = 0. \tag{10}$$

For convenience and following earlier works, diffusion is also assumed to apply within the external mass transfer boundary layer [9,10] as well. However, these results also apply to a convective boundary condition, as discussed further below. Finally, continuity of mass fluxes at the film tips (evaporation front in Fig. 1) reads at steady state

$$\frac{\partial\rho^3}{\partial n} = \mathrm{Ca}_f\frac{\partial\zeta}{\partial n}, \tag{11}$$

where n denotes outer normal.

We proceed as in previous works [11,17] and develop a solution uniformly valid over both film and dry regions by defining the auxiliary variable

$$\Phi = \frac{\rho^3 - 3\mathrm{Bo}_x I + \mathrm{Ca}_f\zeta}{1 + \mathrm{Ca}_f}, \tag{12}$$

where

$$I = \int_0^{\xi}\rho^4 d\xi. \tag{13}$$

This satisfies the Laplace equation over both the film and dry regions as required

$$\nabla^2\Phi = 0 \tag{14}$$

and it is continuous with continuous fluxes at the yet-to-be-determined evaporation front [Eq. (11)]. Equation (14) is then to be solved subject to the following boundary conditions.

(i) At the percolation front ($\xi = \xi_p \leqslant 0$), we have saturated conditions, $\zeta = 1$, $\rho = 1$, hence

$$\Phi = \Phi_p \equiv 1 - \frac{3\mathrm{Bo}_x I(\xi_p)}{1 + \mathrm{Ca}_f}. \tag{15}$$

(ii) At the top of the mass boundary layer outside the porous medium ($\xi = d$), we have $\zeta = 0$, $\rho = 0$, hence

$$\Phi_0 = 0. \tag{16}$$

The unknown position of the film tips is the place where $\rho = 0$ and $\zeta = 1$, hence

$$\Phi = \Phi_i \equiv \frac{\mathrm{Ca}_f}{1 + \mathrm{Ca}_f}. \tag{17}$$

Finally, at the product surface S ($\xi = 0$) mass flux continuity applies

$$\left.\frac{\partial\Phi}{\partial\xi}\right|_{S-} = \lambda\left.\frac{\partial\Phi}{\partial\xi}\right|_{S+}, \tag{18}$$

where $\lambda > 1$ is the ratio of external to effective internal diffusivities. At the same place Φ is discontinuous early in the process. Namely, when the films reach the product surface,

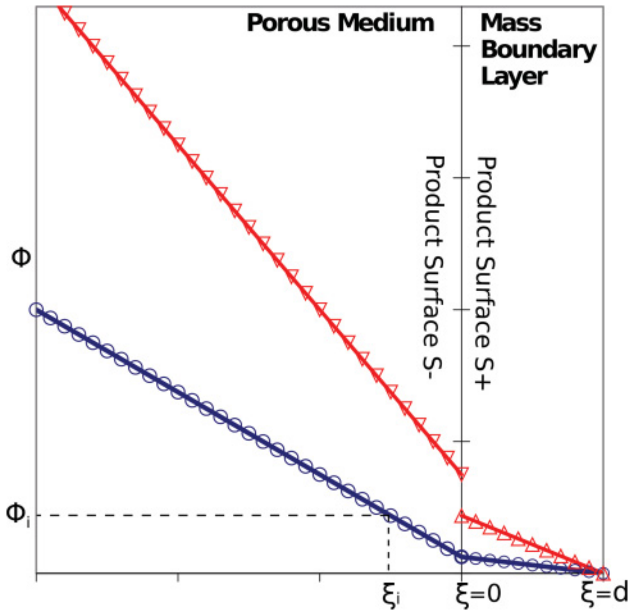

FIG. 2. (Color online) Plot of the auxiliary variable Φ vs the dimensionless depth of the porous medium ξ in the 1D problem. The product surface is located at $\xi = 0$, the percolation front at $\xi_p < 0$ (not shown here) and the film tips at $\xi_i < 0$, where $\Phi(\xi_i) = \mathrm{Ca}_f/(1 + \mathrm{Ca}_f)$. The red line ($\bigtriangledown$) shows a solution for early times when $\xi_p > \xi_{\mathrm{pc}}$, the film tips reach the product surface S, and Φ is discontinuous there. The blue line ($\circ$) shows a solution for later times when $\xi_p \leqslant \xi_{\mathrm{pc}}$, the films have detached from S, and Φ is continuous there.

they have a finite thickness $\rho^* > 0$ on the porous medium side of the surface S–,hence $\Phi(S-) = \frac{\rho^*+\mathrm{Ca}_f}{1+\mathrm{Ca}_f}$, and zero thickness ($\rho = 0$) just over the surface S+, $\Phi(S+) = \frac{\mathrm{Ca}_f}{1+\mathrm{Ca}_f}$. After the detachment of the films, however, Φ becomes continuous at $\xi = 0$.

The 1D solution of Eq. (14) is straightforward: Φ is linear in ξ subject to the above conditions. Schematics of such a solution are shown in Fig. 2 for the two different cases of the film condition at the product surface S. We proceed therefore by considering the two different cases, when gravity opposes or enhances drying, respectively.

III. GRAVITY-OPPOSED DRYING, $\mathrm{Bo}_x = -\mathrm{Bo} \leqslant 0$

Consider, first, the case when gravity opposes drying ($\mathrm{Bo}_x = -\mathrm{Bo}$ and evaporation is from the top). The percolation front is at $\xi_p \leqslant 0$ and the film tips at $\xi_i \leqslant 0$ (where $\xi_i \geqslant \xi_p$). Here and in the material below, we assume that the percolation front has not reached the bottom boundary of the medium, located at $\xi = \xi_b$. This will be relaxed later.

At early stages the films are attached to S ($\rho^* > 0$ at $\xi = \xi_i = 0$). As drying proceeds, ρ^* decreases, and when ξ_p reaches a critical value ξ_{pc} (when $\rho^* = 0$), the films detach. From that point on, the position of the evaporation front recedes within the pore space, $\xi_i < 0$, while a growing dry region forms below the product surface, $\xi_i < \xi \leqslant 0$, where gas-phase diffusion is the controlling process.

A. Films terminate at product surface, $\xi_p > \xi_{\mathrm{pc}}$

When the films end at the external surface S of the porous medium, Φ is discontinuous there,

$$\Phi(S-) = \frac{\rho^{*3} + \mathrm{Ca}_f}{1 + \mathrm{Ca}_f}, \quad \Phi(S+) = \frac{\mathrm{Ca}_f}{1 + \mathrm{Ca}_f}. \tag{19}$$

It is straightforward to show that the solution of Eq. (14) for Φ is

$$\Phi(\xi) = \frac{\mathrm{Ca}_f}{1 + \mathrm{Ca}_f}\left(\frac{d-\xi}{d}\right) \quad \text{for} \quad 0 < \xi \leqslant d, \tag{20}$$

$$\begin{aligned}\Phi(\xi) &= \Phi_p + \frac{\lambda \mathrm{Ca}_f}{1 + \mathrm{Ca}_f}\left(\frac{\xi_p - \xi}{\xi_p}\right)\\ &= \Phi(S-) + \frac{\mathrm{Ca}_f}{1 + \mathrm{Ca}_f}\left(\frac{-\lambda\xi}{d}\right) \quad \text{for} \quad \xi_p \leqslant \xi < 0.\end{aligned} \tag{21}$$

In this regime the mass flux is independent of time and constant

$$-\left.\frac{\partial \Phi}{\partial \xi}\right|_{S+} = \frac{\mathrm{Ca}_f}{d(1 + \mathrm{Ca}_f)} \equiv \frac{\Phi_i}{d}. \tag{22}$$

This defines the CRP regime, which lasts as long as the films stay connected to the surface. The film thickness is obtained by differentiating Eq. (12) and taking $\zeta = 1$

$$\frac{d\rho^3}{d\xi} + 3\mathrm{Bo}\rho^4 = (1 + \mathrm{Ca}_f)\left.\frac{\partial \Phi}{\partial \xi}\right|_{\mathrm{S}-} = -\frac{\lambda \mathrm{Ca}_f}{d}. \tag{23}$$

This can be integrated once

$$\int_{\rho^*}^{\rho} \frac{3\rho^2 d\rho}{\left(\frac{\lambda \mathrm{Ca}_f}{d} + 3\mathrm{Bo}\rho^4\right)} = -\xi. \tag{24}$$

For compactness we will also use the hypergeometric function ${}_2F_1(a,b;c;z)$ to represent the above integral [24]

$$\int_0^z \frac{3u^2}{a + 3bu^4}du = \frac{z^3}{a}\left[{}_2F_1\left(1,3/4;7/4;-3\frac{bz^4}{a}\right)\right]. \tag{25}$$

The thickness of the film is thus

$$\begin{aligned}&\rho^3\left[{}_2F_1\left(1,3/4,7/4,\frac{-3\mathrm{Bo}d}{\lambda\ \mathrm{Ca}_f}\rho^4\right)\right]\\ &\quad - \rho^{*3}\left[{}_2F_1\left(1,3/4,7/4,\frac{-3\mathrm{Bo}d}{\lambda\ \mathrm{Ca}_f}\rho^{*4}\right)\right] = -\frac{\lambda\ \mathrm{Ca}_f}{d}\xi_p,\end{aligned} \tag{26}$$

while the dependence of ρ^* on the position of the percolation front ξ_p can be obtained through

$$\begin{aligned}&{}_2F_1\left(1,3/4,7/4,\frac{-3\mathrm{Bo}d}{\lambda\ \mathrm{Ca}_f}\right)\\ &\quad - \rho^{*3}\left[{}_2F_1\left(1,3/4,7/4,\frac{-3\mathrm{Bo}d}{\lambda\ \mathrm{Ca}_f}\rho^{*4}\right)\right] = -\frac{\lambda\ \mathrm{Ca}_f}{d}\xi_p.\end{aligned} \tag{27}$$

The end of the CRP is at the critical detachment position ξ_{pc}, obtained by setting $\rho^* = 0$ in the above

$$-\frac{\lambda\ \mathrm{Ca}_f}{d}\xi_{\mathrm{pc}} = {}_2F_1\left(1,3/4,7/4,\frac{-3\mathrm{Bo}d}{\lambda\ \mathrm{Ca}_f}\right). \tag{28}$$

Note that the external mass transfer variable occurs in the combination λ/d. It is not difficult to show that more generally it represents an equivalent mass transfer coefficient across the boundary layer. Indeed, if the flux condition at the surface was based instead on a convective mass transfer coefficient h (e.g., Flux $= hC_{S+}$), it can be readily shown that

$$\frac{\lambda}{d} = \mathrm{Sh} \equiv \frac{hr_0}{D_{\mathrm{eff}}} \tag{29}$$

where we defined a Sherwood number Sh for the external mass transfer using the pore length r_0 and the effective internal diffusivity D_{eff} as the characteristic quantities. We remark that because we used the characteristic pore size above, the so-defined Sherwood number would usually take small values. From this point on we will use without loss the equivalence between Sh and d/λ.

It is also worth noting that the explicit effect of Bo can be removed from the above by rescaling all lengths by $-\mathrm{Bo}_x = \mathrm{Bo} > 0$: Then by defining $\hat{\xi} = \mathrm{Bo}\xi$, Eq. (24) becomes independent of Bo

$$\int_{\rho^*}^{\rho} \frac{3\rho^2 d\rho}{(\tau + 3\rho^4)} = -\hat{\xi}, \tag{30}$$

where we introduced the single dimensionless parameter

$$\tau \equiv \frac{\mathrm{ShCa}_f}{\mathrm{Bo}}. \tag{31}$$

One can view τ as an equivalent Rayleigh number $\mathrm{Ra}_{\mathrm{ev}} = \frac{\mathrm{Ca}_f}{\mathrm{Bo}} = \frac{3\pi\beta}{C^*}\frac{C_e D_M \nu}{\rho_l g r_0^3}$ for evaporation in the presence of buoyancy (i.e., $\tau = \mathrm{Ra}_{\mathrm{ev}}\mathrm{Sh}$) where $\nu = \mu/\rho_l$ is viscous diffusivity (as also in the case of miscible fluids [25]). In this notation, the equivalent of Eq. (27) is

$$\begin{aligned} &{}_2F_1\left(1,3/4,7/4,\frac{-3}{\tau}\right) - \rho^{*3}\left[{}_2F_1\left(1,3/4,7/4,\frac{-3}{\tau}\rho^{*4}\right)\right] \\ &\quad = -\tau\hat{\xi}_p \end{aligned} \tag{32}$$

and that of the detachment time $\hat{\xi}_{\mathrm{pc}}$ is

$$\hat{\xi}_{\mathrm{pc}} = -\frac{1}{\tau}\left[{}_2F_1\left(1,3/4,7/4,\frac{-3}{\tau}\right)\right]. \tag{33}$$

Figure 3 shows profiles of the film thickness ρ^* just below the product surface S– as a function of the rescaled position of the percolation front $\hat{\xi}_p$ for different values of τ. The inset of the same figure shows ρ^* vs the position of the percolation front ξ_p for the corresponding values of Bo_x and a fixed value of the capillary number Ca_f. As expected, the film thickness at the product surface decreases as the percolation front recedes in the pore space, higher values of Bo corresponding to shorter films (due to stronger buoyancy) and earlier detachment times (smaller values of the magnitude of ξ_p).

Figure 4 shows the critical rescaled position of the percolation front $\hat{\xi}_{\mathrm{pc}}$ as a function of τ. The figures demonstrate that smaller capillary and Sherwood numbers lead to longer films. The critical percolation front location ξ_{pc} is a slowly increasing function of τ. An asymptotic analysis of the corresponding Eq. (33) shows that at sufficiently large times, namely large values of $-\hat{\xi}_{\mathrm{pc}}$

$$-\hat{\xi}_{\mathrm{pc}} \sim J\tau^{-1/4}, \tag{34}$$

where the algebraic constant J can be expressed in terms of the gamma function $J = 3^{-\frac{3}{4}}\Gamma(1/4)\Gamma(3/4) \simeq 1.462$. This behavior is also demonstrated in Fig. 4. The magnitude of

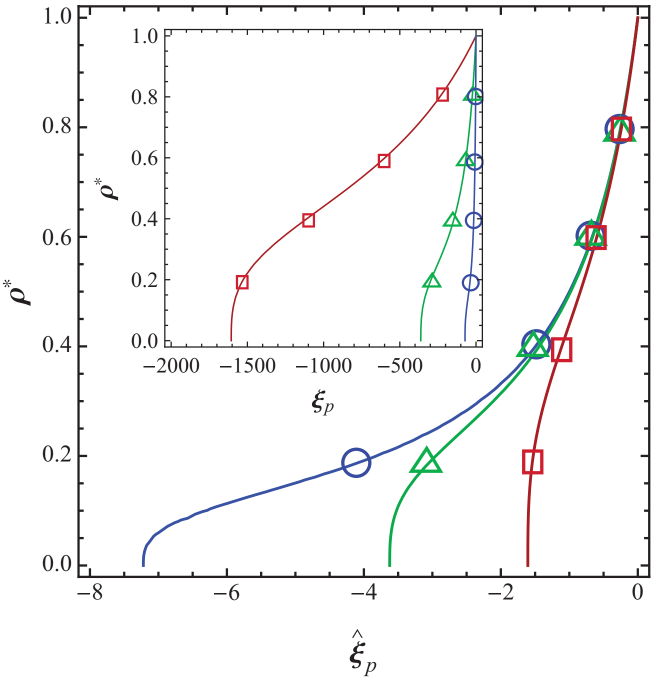

FIG. 3. (Color online) Film thickness ρ^* at the surface vs the rescaled position of the percolation front $\hat{\xi}_p$ for various values of τ; $\tau = 0.1$ (□), $\tau = 0.01$ (△), $\tau = 0.001$ (◯). Inset shows the film thickness at the surface ρ^* vs the position of the percolation front ξ_p for the corresponding values of Bo_x; $\mathrm{Bo}_x = -0.001$ (□), $\mathrm{Bo}_x = -0.01$ (△), $\mathrm{Bo}_x = -0.1$ (◯) when $\mathrm{Ca}_f = 0.001$ and $\mathrm{Sh} = 0.1$. The critical detachment time ξ_{pc} for each case is found when $\rho^* = 0$.

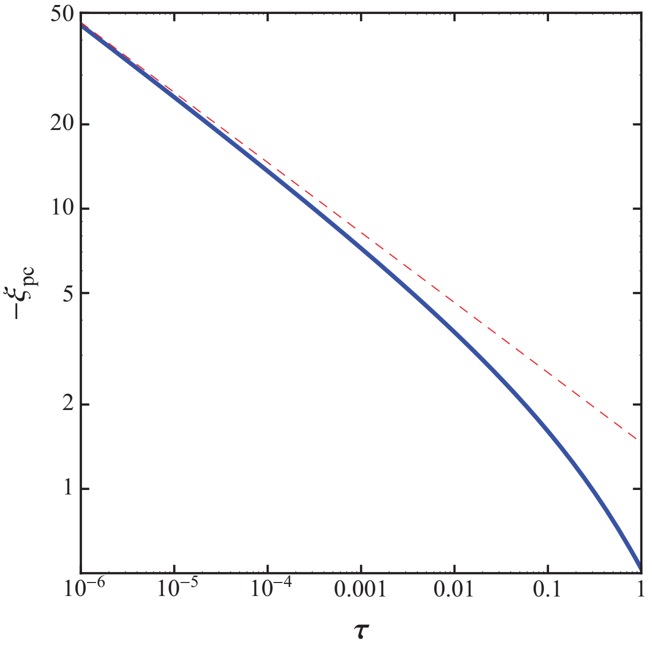

FIG. 4. (Color online) Log-log plot of the rescaled critical detachment position $-\hat{\xi}_{\mathrm{pc}}$ vs τ. The dashed line of slope $-\frac{1}{4}$ corresponds to the asymptotic prediction of Eq. (34).

the percolation front position is used as a proxy for time. Its specific relation to time will be discussed in a later section.

B. Films terminate inside the porous medium, $\xi_p \leqslant \xi_{\mathrm{pc}}$

When the films have detached from S, the evaporation front is at $\xi_i < 0$. Now the variable Φ is continuous at $\xi = 0$ (Fig. 2) and we have

$$\Phi(\xi) = \Phi_i\left(\frac{d-\xi}{d-\lambda\xi_i}\right) = \Phi_p\left(\frac{d-\xi}{d-\lambda\xi_p}\right) \quad \text{for} \quad 0 \leqslant \xi \leqslant d, \tag{35}$$

$$\Phi(\xi) = \Phi_i\left(\frac{d-\lambda\xi}{d-\lambda\xi_i}\right) = \Phi_p\left(\frac{d-\lambda\xi}{d-\lambda\xi_p}\right) \quad \text{for} \quad \xi_p \leqslant \xi \leqslant 0. \tag{36}$$

The drying flux remains proportional to the gradient of Φ and from Eq. (35) we get

$$-\frac{\partial\Phi}{\partial\xi}\bigg|_{+} = \frac{\Phi_i}{d-\lambda\xi_i}. \tag{37}$$

Now the drying rate decreases as ξ_i decreases.

As before, the film thickness ρ is the solution of

$$\frac{d\rho^3}{d\xi} + 3\mathrm{Bo}\rho^4 = (1+\mathrm{Ca}_f)\frac{\partial\Phi}{\partial\xi}\bigg|_{-} = -\frac{\mathrm{ShCa}_f}{1-\mathrm{Sh}\xi_i} \tag{38}$$

or

$$\int_0^{\rho} \frac{3\rho^2 d\rho}{\mathrm{Sh}\frac{\mathrm{Ca}_f}{1-\mathrm{Sh}\xi_i} + 3\mathrm{Bo}\rho^4} = \xi_i - \xi \tag{39}$$

and in compact notation,

$$\rho^3\left[{}_2F_1\left(1,3/4,7/4,-3\rho^4\mathrm{Bo}\frac{1-\mathrm{Sh}\xi_i}{\mathrm{ShCa}_f}\right)\right] = \frac{\mathrm{ShCa}_f}{1-\mathrm{Sh}\xi_i}(\xi_i-\xi). \tag{40}$$

By taking $\rho = 1$ at $\xi = \xi_p$, we obtain ξ_i as a function of ξ_p

$${}_2F_1\left(1,3/4,7/4,-3\mathrm{Bo}\frac{1-Sh\xi_i}{\mathrm{ShCa}_f}\right) = \frac{\mathrm{ShCa}_f}{1-\mathrm{Sh}\xi_i}(\xi_i-\xi_p). \tag{41}$$

With the percolation front location as a proxy for time, we can determine all relevant variables, including the location of the film tips ξ_i, as well as the film thickness profiles over ξ. However, in this regime the effect of Bo cannot be simply rescaled out as before, except for the critical percolation time. Indeed, by using the rescaled notation, the above become

$$\rho^3\left[{}_2F_1\left(1,3/4,7/4,-3\rho^4\frac{\mathrm{Bo}-\mathrm{Sh}\hat{\xi}_i}{\mathrm{Bo}\tau}\right)\right] = \frac{B\tau}{\mathrm{Bo}-\mathrm{Sh}\hat{\xi}_i}(\hat{\xi}_i-\hat{\xi}), \tag{42}$$

and

$${}_2F_1\left(1,3/4,7/4,-3\frac{\mathrm{Bo}-\mathrm{Sh}\hat{\xi}_i}{\mathrm{Bo}\tau}\right) = \frac{\mathrm{Bo}\tau}{\mathrm{Bo}-\mathrm{Sh}\hat{\xi}_i}(\hat{\xi}_i-\hat{\xi}_p). \tag{43}$$

The profile for ρ as a function of ξ is plotted in Fig. 5 for various values of the dimensionless numbers Bo and Ca_f. The familiar cubic dependence as the film tip is approached is evident [11]. For larger values of Bo, the liquid films become shorter as buoyancy forces increasingly dominate over capillary forces and the films detach from the product surface earlier [Fig. 5 (left)]. The effect of Ca_f is demonstrated in

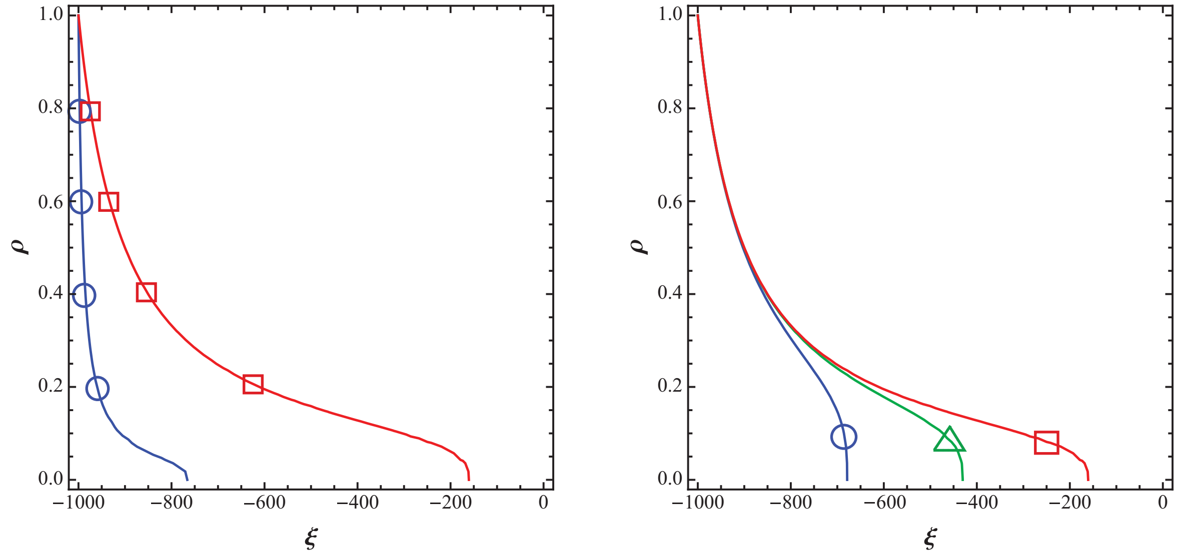

FIG. 5. (Color online) (Left) Film profile ρ vs ξ for a fixed position of the percolation front $\xi_p = -1000$ ($\xi_p \leqslant \xi_{\mathrm{pc}}$) for different values of the bond number; $\mathrm{Bo}_x = -0.1$ (○) and $\mathrm{Bo}_x = -0.01$ (□) when $\mathrm{Ca}_f = 0.001$ and $\mathrm{Sh} = 0.1$. (Right) Film profile ρ vs ξ for the same fixed position of the percolation front for different values of the capillary number; $\mathrm{Ca}_f = 0.1$ (○), $\mathrm{Ca}_f = 0.01$ (△), and $\mathrm{Ca}_f = 0.001$ (□) when $\mathrm{Bo}_x = -0.01$ and $\mathrm{Sh} = 0.1$.

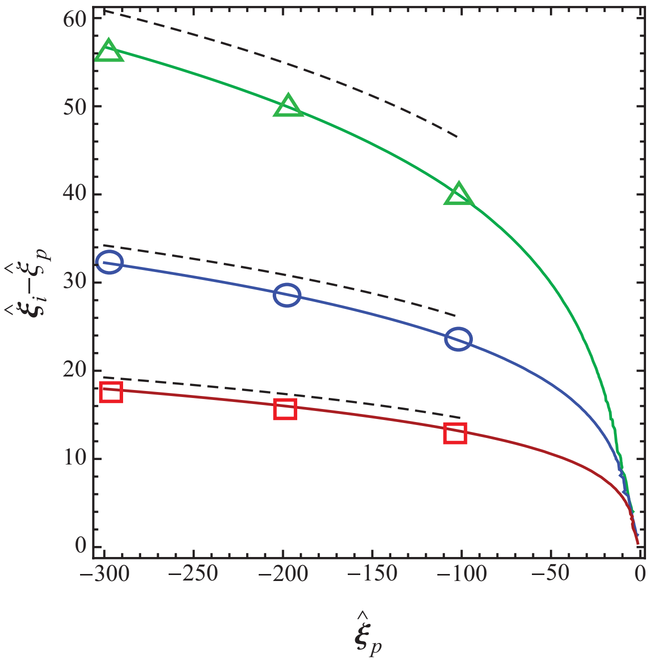

FIG. 6. (Color online) The rescaled spatial extent of the film region $\hat{\xi}_i - \hat{\xi}_p$ as a function of the rescaled position of the percolation front $\hat{\xi}_p$ for different values of the parameter τ and Bo/Sh = 0.01; $\tau = 1$ (□), $\tau = 0.1$ (○), $\tau = 0.01$ (△). The dashed lines correspond to the asymptotic dependence of Eq. (44) at large values of $-\hat{\xi}_p$.

Fig. 5 (right), with smaller values of Ca_f leading to longer films as capillarity dominates over viscosity supporting liquid flow over longer distances in the porous medium. This results in later detachment times and a longer CRP that eventually leads to faster drying of the medium.

Figure 6 shows the rescaled extent of the film region $\hat{\xi}_i - \hat{\xi}_p$ as a function of the rescaled percolation front position $\hat{\xi}_p$ for various values of the dimensionless parameter τ. All curves collapse to the same curve at early times, but increasingly deviate later, when the two fronts appear to be separated by only a slowly varying distance, which is the film region extent and which is smaller as τ is larger. An asymptotic analysis of Eq. (43) shows that at sufficiently large times, namely $-\hat{\xi}_p \gg 1$, we have

$$-\hat{\xi}_p \sim \frac{\mathrm{Ca}_f}{J^4}(\hat{\xi}_i - \hat{\xi}_p)^4 = \frac{\tau \mathrm{Bo}}{\mathrm{Sh} J^4}(\hat{\xi}_i - \hat{\xi}_p)^4, \tag{44}$$

which is apparent in Fig. 6.

Before closing this section we note that the previous analysis must be modified when the percolation front reaches the lower boundary. Then the bulk liquid region, providing liquid for the films, no longer exists and the remaining fluid is contained only in the film region. The boundary condition corresponding to the percolation front must now be replaced by its counterpart $\Phi = (\rho_b^3 + 3\mathrm{Bo} I_b + \mathrm{Ca}_f)/(1+\mathrm{Ca}_f)$ at $\xi_p = \xi_b$ and the control parameter for evaporation is either the film thickness ρ^* at $\xi = 0$ or the thickness ρ_b at $\xi = \xi_b$. Again we need to distinguish two cases, depending on whether the films detach from the product surface prior to or after the percolation front reaches the bottom of the medium. In the first case, where $\xi_b \leqslant \xi_{\mathrm{pc}}$, Eq. (42) is still valid provided we set $\rho = \rho_b$ at $\xi = \xi_b$, hence

$$\rho_b^3\left[{}_2F_1\left(1,3/4,7/4,-3\rho_b^4\frac{\mathrm{Bo}-\mathrm{Sh}\hat{\xi}_i}{\mathrm{Bo}\tau}\right)\right] = \frac{\mathrm{Bo}\tau}{\mathrm{Bo}-\mathrm{Sh}\hat{\xi}_i}(\hat{\xi}_i - \hat{\xi}_b). \tag{45}$$

In the second case, where $\xi_b > \xi_{\mathrm{pc}}$, it is Eq. (26) that is valid with $\rho = \rho_b$ at $\xi_p = \xi_b$

$$\rho_b^3\left[{}_2F_1\left(1,3/4,7/4,-3\frac{\rho_b^4}{\tau}\right)\right] - \rho^{*3}\left[{}_2F_1\left(1,3/4,7/4,-3\frac{\rho^{*4}}{\tau}\right)\right] = -\tau\hat{\xi}_b. \tag{46}$$

The corresponding expression for the flux, $\partial\Phi/\partial\xi$, remains the same as do the evaporation rate expressions.

C. The drying curve

We proceed now by determining the drying curve. The dimensional drying rate is obtained from its dimensionless counterpart through the solution for variable Φ

$$\dot{\Im} = -\frac{D_M r_0^2 C_e (1+\mathrm{Ca}_f) N_y N_z}{\mathrm{Ca}_f}\left.\frac{d\Phi}{d\xi}\right|_{S+}, \tag{47}$$

where N denotes size. Its constant value at the onset of the process during the CRP will be used to normalize all rates

$$\dot{\Im}_{\mathrm{CRP}} = D_M r_0^2 C_e N_y N_z \frac{1}{d}, \tag{48}$$

hence

$$E = \frac{\dot{\Im}}{\dot{\Im}_{\mathrm{CRP}}} = \frac{1}{1-\mathrm{Sh}\xi_i} = \frac{\mathrm{Bo}}{\mathrm{Bo}-\mathrm{Sh}\hat{\xi}_i}. \tag{49}$$

This provides a direct relationship between drying rates and the position of the film tips ξ_i, and through the relationship of the latter to the percolation front position ξ_p. To connect the variables to the process time, we will derive expressions for the overall liquid volumetric content, which we will denote as the liquid saturation, S_{res}. This is the combined sum of the bulk liquid in the pores below the percolation front and that contained in the liquid films. The bulk fluid contribution is $4(\xi_p - \xi_b)$ assuming $\xi_p \geqslant \xi_b$. The amount in the films S_f is obtained by integrating the cross sectional area of the film region $\xi_i - \xi_p$, which is proportional to ρ^2, hence

$$S_f = -C^* \int_{\xi_i}^{\xi_p} \rho^2 d\xi. \tag{50}$$

During the CRP we have

$$\begin{aligned} S_f &= C^* \int_{\rho^*}^{1} \frac{3\rho^4 d\rho}{\mathrm{Sh}\mathrm{Ca}_f + 3\mathrm{Bo}\rho^4} \\ &= \frac{C^*}{\mathrm{Bo}}\left[1 - {}_2F_1\left(1,1/4,5/4,-\frac{3}{\tau}\right)\right] \\ &\quad - \rho^* \frac{C^*}{\mathrm{Bo}}\left[1 - {}_2F_1\left(1,1/4,5/4,-\frac{3}{\tau}\rho^{*4}\right)\right], \end{aligned} \tag{51}$$

while following detachment (during the FRP),

$$S_f = C^*\int_0^1 \frac{3\rho^4 d\rho}{\frac{\mathrm{ShCa}_f}{1-\mathrm{Sh}\xi_i} + 3\mathrm{Bo}\rho^4} = \frac{C^*}{\mathrm{Bo}}\left[1 - {}_2F_1\left(1,1/4,5/4,-\frac{3}{\tau E}\right)\right], \quad (52)$$

where we used Eq. (49). The overall liquid saturation, S_{res}, is

$$S_{\mathrm{res}} = \frac{4(\xi_p - \xi_b) + S_f}{-4\xi_b}. \quad (53)$$

The above equations relate implicitly the position of the percolation front ξ_p to the remaining liquid saturation. The relation to time results from the mass balance

$$\frac{dS_{\mathrm{res}}}{dt} = -E. \quad (54)$$

The above are valid before the percolation front reaches the bottom of the medium. After that condition is reached, the film thickness is obtained from Eqs. (45) and (46) and a similar procedure can be applied. For simplicity, details will be omitted.

The drying curve is a plot of the normalized evaporation flux E versus the liquid saturation S_{res}. By using the previous expressions we construct the plots shown in Fig. 7 that demonstrate the shape of the drying curve for different values of Bo and fixed values of Ca_f and Sh. The curves show a clear CRP, where $E = 1$, at early times (higher values of liquid saturation S_{res}) that lasts until the films detach from the product surface S (when the percolation front reaches ξ_{pc}). The plot shows that the CRP is shorter for higher values of the bond number that corresponds to stronger buoyancy effects within the films. After that time, the drying rate decreases rapidly as a completely dry region of increasing extent develops between the evaporation front ξ_i and the product surface. This regime corresponds to the FRP. A last regime occurs at very low residual saturations, when the percolation front reaches the bottom of the medium, and the bulk liquid has evaporated. This regime corresponds to the shrinking of the liquid films and is particularly evident for higher values of Bo. It is also interesting to note that the dimensionless drying rate E has a value slightly greater than zero at the limit $S_{\mathrm{res}} \to 0$ that corresponds to an evaporation front ξ_i located exactly at the bottom of the medium ξ_b, namely $E_{\mathrm{min}} = \frac{1}{1-\mathrm{Sh}\xi_b}$.

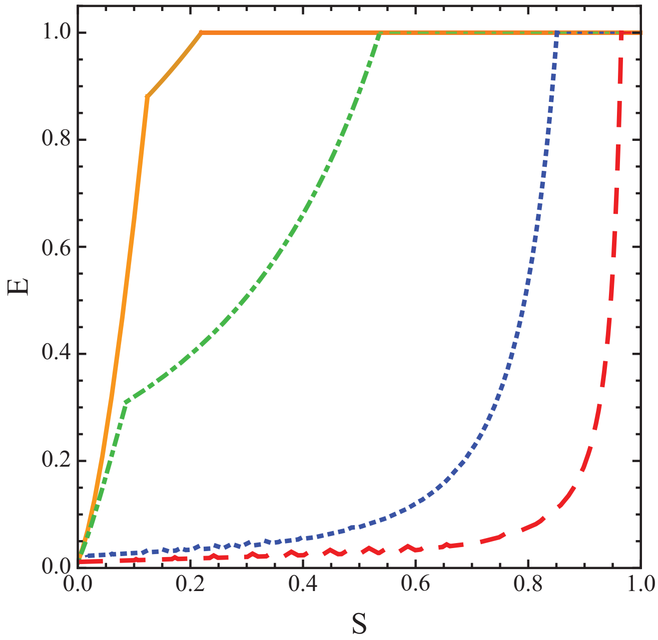

FIG. 7. (Color online) Dimensionless drying rate E as a function of the liquid saturation S_{res} for different values of the bond number [$\mathrm{Bo}_x = -0.1$ (red-dashed line); $B_x = -0.01$ (blue-dotted line); $\mathrm{Bo}_x = -0.001$ (green-dot-dashed line); $\mathrm{Bo}_x = -0.0001$ (orange-continuous line)] for $\mathrm{Ca}_f = 0.01$, $\mathrm{Sh} = 0.1$, and $\xi_b = -1000$. The smaller the effect of gravity, the longer the CRP. The curves correspond to a solution where the films detach from the product surface before the percolation front reaches the bottom of the medium, namely when $\xi_{\mathrm{pc}} \geqslant \xi_b$. Note the difference in the curves at lower bond numbers as the bottom boundary is approached.

Of importance is the critical saturation S^c_{res} when the CRP regime ends, namely when the surface film thickness becomes $\rho^* = 0$ for the first time. Its value depends on whether the films detach from the surface before ($\xi_b \leqslant \xi_{\mathrm{pc}}$) or after ($\xi_b > \xi_{\mathrm{pc}}$) the percolation front has reached the bottom boundary ξ_b. After calculations, omitted for simplicity, we find

$$S^c_{\mathrm{res},1} = 1 + \frac{1}{\tau\hat{\xi}_b}\left[{}_2F_1\left(1,3/4,7/4,-\frac{3}{\tau}\right)\right] - \frac{C^*}{4\hat{\xi}_b}\left[1 - {}_2F_1\left(1,1/4,5/4,-\frac{3}{\tau}\right)\right], \quad (55)$$

in the first case, and

$$S^c_{\mathrm{res},2} = -\frac{\mathrm{Bo}S_f}{4\hat{\xi}_b} = -\frac{C^*\rho_b}{4\hat{\xi}_b}\left[1 - {}_2F_1\left(1,1/4,5/4,-\frac{3\rho_b^4}{\tau}\right)\right], \quad (56)$$

where ρ_b is given by

$$\rho_b^3\,{}_2F_1\left(1,3/4,7/4,-\frac{3\rho_b^4}{\tau}\right) = -\tau\hat{\xi}_b \quad (57)$$

in the second. As expected, if the medium is infinitely long, the critical saturation is equal to 1. Figure 8 shows the critical saturation for various values of τ for this case. As expected the critical saturation parameter is a strong function of τ.

IV. GRAVITY-ENHANCED DRYING, $\mathrm{Bo}_x = \mathrm{Bo} > 0$

A. 1D predictions

The previous analysis was developed under the condition that gravity opposes liquid flow through the films where a 1D effective continuum solution is valid. This may not necessarily be the case when film flow is enhanced by gravity ($B_x > 0$). Under this condition and for sufficiently strong buoyancy, both the percolation and the evaporation front are likely to become unstable, mass transfer through the porous medium will not be sufficiently fast to balance gravity and establish a quasi-1D regime, and the films will remain at the product surface for very

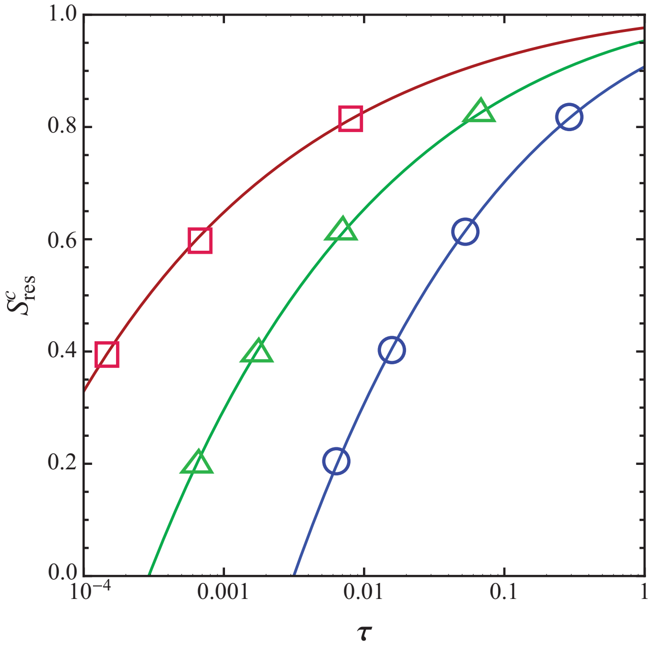

FIG. 8. (Color online) Critical saturation S^c_{res} vs parameter τ when the films detach before the percolation front reaches the bottom of the medium ($\hat{\xi}_b < \hat{\xi}_{\mathrm{pc}}$) for various values of $\hat{\xi}_b$; $\hat{\xi}_b = -20$ (□), $\hat{\xi}_b = -10$ (△), $\hat{\xi}_b = -5$ (◯). From the solution of Eq. (55).

long times leading to longer CRPs and a faster recovery of the liquid. In the case, however, that gravity is not so strong, it is possible that mass transfer can be sufficiently fast to convect the gravity-draining liquid through the films and establish a flow regime that can be approached with the previous methods.

To determine if such a regime exists we consider the 1D analysis of the previous section for $\mathrm{Bo}_x > 0$. In this case films will stay at the product surface S provided that a solution of the following equation, which is the counterpart of Eq. (24) for $\mathrm{Bo}_x > 0$, exists:

$$\int_{\rho^*}^{1} \frac{3\rho^2 d\rho}{\mathrm{ShCa}_f - 3\mathrm{Bo}\rho^4} = -\xi_p. \tag{58}$$

Clearly, a necessary condition is that the integral does not diverge, which is satisfied if

$$\mathrm{ShCa}_f > 3\mathrm{Bo} \Rightarrow \tau > 3. \tag{59}$$

This condition is favored by stronger viscous forces (compared to gravity) and faster mass transfer in the dry region and over the product surface. Then, a solution to Eq. (24) exists and can be computed as in the previous sections. The resulting surface film thickness ρ^* at the surface as a function of the percolation front position ξ_p is shown in Fig. 9 for the case of gravity-enhanced drying ($\mathrm{Bo}_x > 0$), and the cases of zero gravity ($\mathrm{Bo}_x = 0$) and gravity-opposed drying ($\mathrm{Bo}_x < 0$). The solution for $\rho^* = 0$ gives the critical position of the percolation front ξ_{pc}. Larger values of Bo_x lead to later detachment times and evidently longer CRPs.

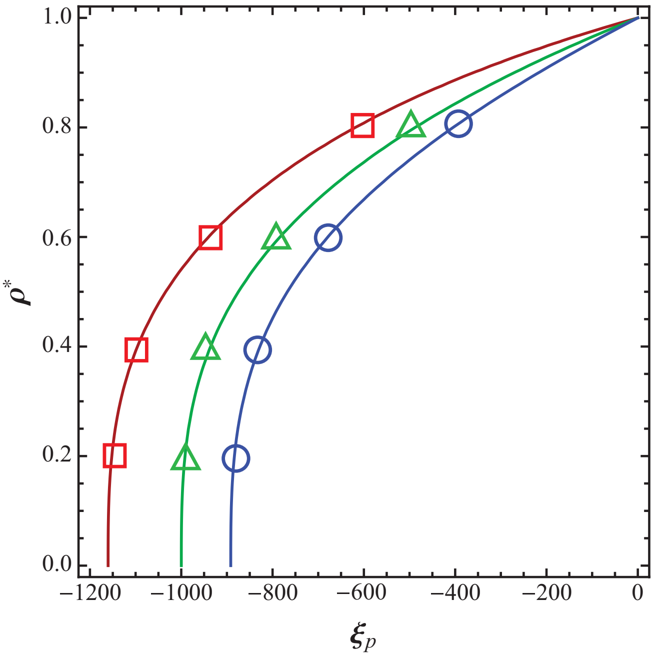

FIG. 9. (Color online) Film thickness ρ^* as a function of the position of the percolation front ξ_p for the case of gravity-enhanced drying, $\mathrm{Bo}_x = 0.0001$ (□), when gravity is neglected, $\mathrm{Bo}_x = 0$ (△), and when it opposes drying, $\mathrm{Bo}_x = -0.0001$ (◯). The CRP lasts longer when $\mathrm{Bo}_x > 0$ as expected. $\mathrm{Ca}_f = 0.01$, $\mathrm{Sh} = 0.1$.

After the films detach, and always under the condition of Eq. (59), their thickness is obtained through equation

$$\int_{0}^{\rho} \frac{3\rho^2 d\rho}{\left(\frac{\mathrm{ShCa}_f}{1-\mathrm{Sh}\xi_i} - 3\mathrm{Bo}\rho^4\right)} = \xi_i - \xi. \tag{60}$$

As the magnitude of ξ_i increases, however, the above integral will diverge when the following condition is approached

$$-\xi_{is} = \frac{\left(\frac{\tau}{3} - 1\right)}{\mathrm{Sh}} \quad \text{or} \quad H = \frac{\pi\beta}{C^*}\frac{D_M C_e v}{\rho g r_0^2} - \frac{D}{\lambda}, \tag{61}$$

where $H = (-\xi_{is})r_0$ and $D = dr_0$ are the dimensional position and boundary layer thickness, respectively. This implies that the evaporation front will become stationary at that location. Inspection of Eq. (61) shows that this location consists of two competing terms; one due to gravity involving τ, which does not depend on surface tension, and another corresponding to external mass transfer. Under the condition that diffusivity within the medium and viscous forces are strong enough to balance gravity, or that external mass transfer is not very strong, films will detach and their tips will stabilize at a fixed location. Such behavior is indeed demonstrated in Fig. 11. The location of the evaporation front ξ_i reaches a stationary state at sufficiently large values of time (position of the percolation front ξ_p) (inset of Fig. 11). It is interesting to note that the film thickness profile in Fig. 10 is qualitatively different from that of gravity-opposed drying. The film thickness becomes almost constant and equal to unity away from the film tips, and decreases rapidly to zero as that position ξ_i is approached.

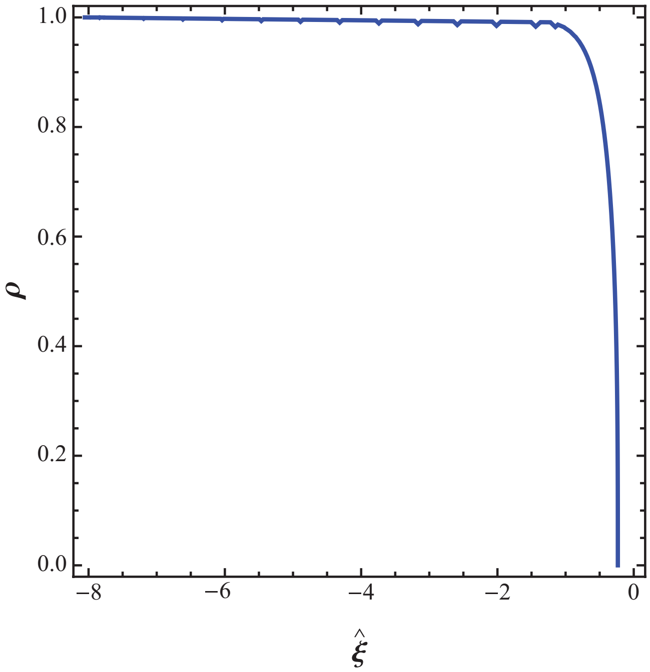

FIG. 10. (Color online) Plot of the film thickness ρ vs $\hat{\xi}$ for the case of gravity-enhanced drying when Bo/Sh $= 0.1$, $\mathrm{Ca}_f = 1$ and $\hat{\xi_p} = -8$. The film thickness remains practically constant and equal to unity along the entire length of the film region, except very close to the film tips $\hat{\xi}_i$, where it decreases sharply to zero.

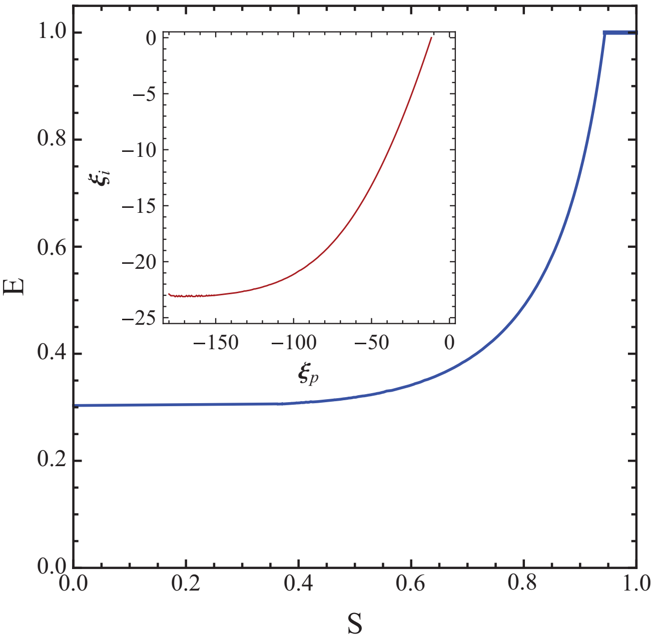

FIG. 11. (Color online) Drying curve for the unstable case, $\mathrm{Bo}_x > 0$, under the condition $\tau > 3$. The curve clearly exhibits two CRP regimes: an early one that lasts until the films detach from the product surface S–and a late one that occurs when the condition of Eq. (61) is satisfied. $\mathrm{Ca}_f = 1.0$, $\mathrm{Bo}_x = 0.01$, $\mathrm{Sh} = 0.1$, and $\xi_b = -180$. Inset shows the corresponding position of the evaporation front ξ_i as a function of the position of the percolation front ξ_p. The stationary state solution for ξ_i corresponds to the solution of Eq. (61).

This practically implies that the flow through the films is driven by gravity, rather that capillarity-induced pressure gradients, since the term $\frac{\partial r^3}{\partial x} \simeq 0$ in Eq. (3).

The above analysis suggests that when the evaporation front reaches the stationary state, the drying curve should exhibit a second period of constant drying rate (following the initial CRP and FRP) when the dimensionless drying rate becomes equal to $E = \frac{3}{\tau}$. This behavior is indeed demonstrated in Fig. 11.

B. Linear stability analysis of buoyant instability of an evaporation front

While the previous analysis showed that a stationary front for the film tips is possible for a percolation front that continuously recedes deeper in the pore space, it cannot indicate whether it is in fact stable. To verify its stability we consider a somewhat simpler approach in the absence of films, as shown in right side of Fig. 12. In this model, liquid (darker gray) drains downward due to gravity in a porous medium of porosity ϕ and permeability k. At a finite location $z = -H$, it evaporates and then diffuses through the medium (lighter gray region) toward the outside of the medium where it is purged at the mass boundary layer (white region). The concentration of the liquid vapors is zero at $z = D$. We will find the stationary states of this process and their stability.

Here we introduce the following dimensionless notation, where all lengths are normalized with H, concentration with C_e, pressure with $\rho g H$, fluid velocity with $k\rho g/\mu$, and time with $\phi H \mu / k\rho g$. The evaporation front is considered at location

$$\Upsilon \equiv z - f(y,t). \tag{62}$$

The relevant dimensionless Darcy's law, continuity and diffusion equations are respectively

$$\vec{u} = -\vec{\nabla} p + \vec{i}, \tag{63}$$

$$\vec{\nabla} \cdot \vec{u} = 0, \quad \text{and} \tag{64}$$

$$\nabla^2 \zeta = 0, \tag{65}$$

where $\vec{i}$ is the unit vector in the downward direction.

At the interface the liquid pressure is assumed zero (equal to the surrounding constant gas pressure and in the absence of capillary or surface tension effects) and the mass balance reads

$$u_n + \mathrm{Ra_k} \frac{\partial \zeta}{\partial n} = \phi v_n \equiv -\Upsilon_t / |\vec{\nabla} \Upsilon|, \tag{66}$$

where $\mathrm{Ra_k} = \frac{C_e D_M \nu}{\rho_l g k H}$ is analogous to the above-defined number for evaporation in porous medium and v_n is the normal component of the interface velocity. At the product surface $z = 0$, we have continuity of concentration and mass fluxes, and at $z = d_s$, $\zeta = 0$.

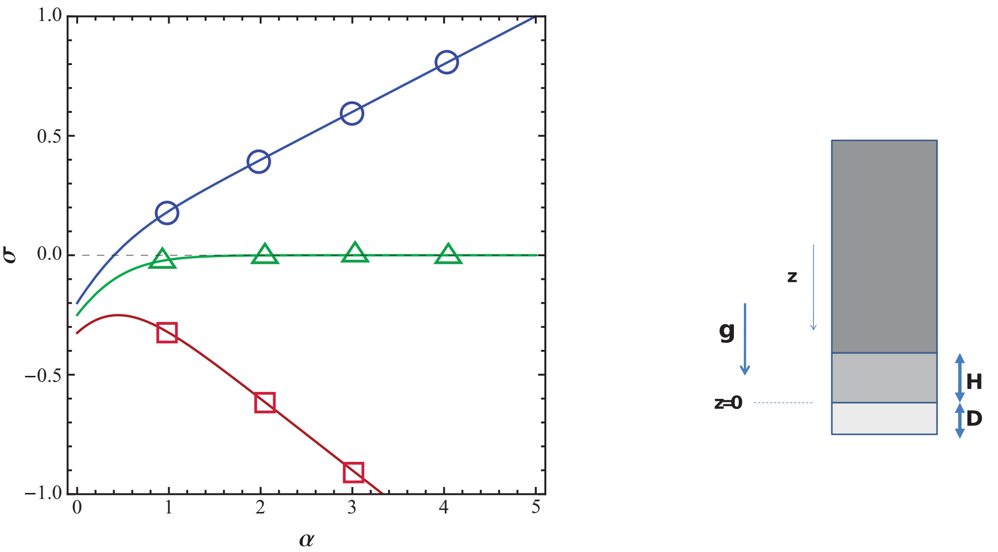

FIG. 12. (Color online) (Left) Dispersion relation of the linear stability analysis for various values of $\mathrm{Ra_k}$ and $\lambda = 1$; $d_s = 1$. $\mathrm{Ra_k} = 0.8$ (◯), $\mathrm{Ra_k} = 1$ (△), and $\mathrm{Ra_k} = 1.3$ (□). For $\mathrm{Ra_k} > 1$ the condition of Eq. (73) is always fulfilled. (Right) Schematic of the process for the linear stability analysis of an evaporation front in the presence of gravity with $\mathrm{Bo}_x > 0$. Liquid (darker gray region) drains downwards due to gravity and evaporates at position $z = -H$. It then diffuses through the porous medium and the mass boundary layer (lighter gray regions). The concentration of the liquid vapors is zero at $z = D$.

The properties of the stationary state are easily derived;

$$f = -1; \quad p_0 = \left(1 - \frac{\lambda \mathrm{Ra_k}}{\lambda + d_s}\right)(z+1);$$
$$\zeta_0 = 1 - \frac{\lambda(z+1)}{\lambda + d_s}; \quad -1 < z < 0; \tag{67}$$
$$\zeta_0 = \frac{d_s - z}{\lambda + d_s}; \quad 0 < z < d_s.$$

Importantly, this state requires that the liquid viscous flow rate is balanced by evaporation and diffusion into the surroundings. Expressed in terms of dimensional variables this condition reads

$$H = \frac{D_M C_e \nu}{k\rho g} - \frac{D}{\lambda}. \tag{68}$$

Note the similarity of Eq. (68) to those of the stationary evaporation front, Eq. (61). Again, we note that the stationary front consists of two counterbalancing terms, one due to gravity and the other due to mass transfer. If gravity is sufficiently small, namely when

$$\mathrm{ShRa_k}\frac{H}{r_0} > 1, \tag{69}$$

then a balance and a stationary state exists within the porous medium. The above condition is analogous to the condition $\tau > 3$, derived for the more general problem that accounts also for the liquid films.

For a linear stability analysis, we next take small (ϵ) perturbations at the front, of wave vector α and temporal growth rate σ

$$f(y,t) = -1 + \epsilon \exp(i\alpha y + \sigma t) \tag{70}$$

and corresponding perturbations on the pressure and concentration. These are substituted and linearized in Eqs. (62) and (63) and the boundary conditions of Eq. (66). After tedious calculations, we obtain the linears stability dispersion relation for the rate of growth as a function of the wave number

$$\sigma = \left(1 - \frac{\lambda \mathrm{Ra_k}}{\lambda + d_s}\right)\alpha - \left(\frac{\lambda \mathrm{Ra_k}}{\lambda + d_s}\right) \times \frac{\sinh \alpha d_s \sinh \alpha + \lambda \cosh \alpha d_s \cosh \alpha}{\sinh \alpha d_s \cosh \alpha + \lambda \cosh \alpha d_s \sinh \alpha}\alpha, \tag{71}$$

which is plotted in Fig. 12. As can be shown analytically, the long-wave (small wave number) (LW) limit is stable, whereas the short-wave (SW) limit could be either stable or unstable

$$\sigma_{\mathrm{LW}} = -\frac{\lambda^2 \mathrm{Ra_k}}{(\lambda + d_s)^2}; \quad \sigma_{\mathrm{SW}} = \left(1 - \frac{2\lambda \mathrm{Ra_k}}{\lambda + d_s}\right)\alpha. \tag{72}$$

The condition for stability is therefore

$$2\mathrm{Ra_k} > 1 + \frac{d_s}{\lambda}. \tag{73}$$

Using Eq. (68) for H, the above reads

$$\mathrm{Ra_k} > 0, \tag{74}$$

which is always satisfied. We conclude, therefore, that if the condition of Eq. (69) is satisfied, the evaporation front is stable. By extension, we believe that the same applies to the general case described in the previous section under the condition $\tau > 3$.

V. CONCLUSION

We have presented a mathematical model for the drying of porous media that accounts for capillarity-induced flow through liquid films, the effect of gravity on the extent of the film region, and mass transport through an external mass boundary layer over the medium surface. By treating the medium as a 1D continuum in the case when gravity opposes drying, thus leading to a stable percolation front, we obtain analytical expressions for all relevant variables, such as the drying rates and the critical saturation that marks the transition from the constant to the falling rate periods. Based on these expressions, we study the effect of capillarity (expressed as a film-based capillary number) and gravity (through the bond number). In such cases, gravity opposes drying and leads to a shorter CRP regime, shorter films, and reduction of the overall drying rate. When gravity enhances film flow, the analytical results are valid only when a suitably defined Rayleigh number is sufficiently large to stabilize the front. This condition is qualitatively similar to a condition obtained by considering the linear stability analysis of a simpler 2D problem. We find that in the latter case, there exists a solution where the evaporation front reaches a stationary state, thus leading to a second constant rate period regime that occurs after the films detach from the medium surface. The detailed analysis of the destabilizing case will be the subject of a pore-network study to be presented, along with supporting experimental results in future work.

ACKNOWLEDGMENTS

The work of A.G.Y. is supported by the EU funded Grant Real Pore Flows, Contract No. 254804 under call FP7-PEOPLE-IEF2009, the contribution of which is gratefully acknowledged. Funding was also provided by the Initial Training Network Multiflow, Contract No. GA-2008-214919. The authors acknowledge the assistance of Mrs. Dora Kotzampasi.

---

[1] J. van Brakel, *in Advances in Drying Vol. 1*, edited by A. Mujumdar (Hemisphere Publishing Co., 1980).
[2] J. Laurindo and M. Prat, Chem. Eng. Sci. **53**, 2257 (1998).
[3] T. Ransohoff and C. Radke, J. Colloid Interface Sci. **121**, 392 (1988).
[4] M. Dong and I. Chatzis, J. Colloid Interface Sci. **172**, 278 (1995).
[5] J. C. T. Eijkel, B. Dan, H. W. Reemeijer, D. C. Hermes, J. G. Bomer, and A. van den Berg, Phys. Rev. Lett. **95**, 256107 (2005).
[6] P. Lehmann, S. Assouline, and D. Or, Phys. Rev. E **77**, 056309 (2008).
[7] N. Shokri, P. Lehmann, P. Vontobel, and D. Or, Water Resour. Res. **44** W06418 (2008).
[8] P. Faure and P. Coussot, Phys. Rev. E **82**, 036303 (2010).
[9] M. Suzuki and S. Maeda, J. Chem. Eng. Jpn. **1**, 26 (1968).
[10] A. G. Yiotis, I. N. Tsimpanogiannis, A. K. Stubos, and Y. C. Yortsos, Water Resour. Res. **43** W06403 (2007).
[11] A. Yiotis, A. G. Boudouvis, A. K. Stubos, I. N. Tsimpanogiannis, and Y. C. Yortsos, Phys. Rev. E **68**, 037303 (2003).
[12] N. Shokri, P. Lehmann, and D. Or, Water Resour. Res. **45**, W10433 (2009).
[13] N. Shokri, P. Lehmann, and D. Or, Geophys. Res. Lett. **35**, L19407 (2008).
[14] I. Fatt, Trans. AIME **207**, 144 (1956).
[15] M. Prat, Int. J. Multiphase Flow **19**, 691 (1993).
[16] M. Prat, Int. J. Multiphase Flow **21**, 875 (1995).
[17] A. Yiotis, A. Boudouvis, A. Stubos, I. Tsimpanogiannis, and Y. Yortsos, AIChE J. **50**, 2721 (2004).
[18] M. Prat, Int. J. Heat Mass Transf. **50**, 1455 (2007).
[19] F. Chauvet, P. Duru, S. Geoffroy, and M. Prat, Phys. Rev. Lett. **103**, 124502 (2009).
[20] F. Chauvet, P. Duru, and M. Prat, Phys. Fluids **22**, 112113 (2010).
[21] A. Yiotis, D. Salin, E. Tajer, and Y. Yortsos (unpublished).
[22] D. Wilkinson, Phys. Rev. A **30**, 520 (1984).
[23] J. F. Gouyet, M. Rosso, and B. Sapoval, Phys. Rev. B **37**, 1832 (1988).
[24] M. Abramowitz and I. Stegun, *Handbook of Mathematical Functions, With Formulas, Graphs, and Mathematical Tables* (US Government Printing Office, Washington, D.C., 1964).
[25] J. Martin, N. Rakotomalala, and D. Salin, Phys. Fluids **14**, 902 (2002).